

# Non-unitary versus unitary optimization in the control of open quantum systems

Marllos E. Fonseca,<sup>1</sup> Felipe F. Fanchini,<sup>2</sup> Emanuel F. de Lima,<sup>1</sup> and Leonardo K. Castelano<sup>1,\*</sup>

<sup>1</sup>*Departamento de Física, Universidade Federal de São Carlos (UFSCar)  
São Carlos, SP 13565-905, Brazil*

<sup>2</sup>*Faculty of Sciences, UNESP - São Paulo State University, 17033-360 Bauru, São Paulo, Brazil*  
(Dated: June 14, 2023)

In this work, we compare the performance of the Krotov method for open quantum systems (non-unitary optimization) with the Krotov method for closed quantum systems (unitary optimization) in finding optimal controls aimed at manipulating qubits and qutrits in the presence of the environment. In the case of unitary optimization, the Krotov method is applied to quantum system neglecting its interaction with the environment, afterwards the resulting controls are used to manipulate the system along with the environmental noise. We consider two distinct control problems: target-state preparation from a given initial state and quantum gate implementation. For the state preparation, we have found that the performance of the controls obtained from the non-unitary optimization outperform that of the controls obtained from the unitary optimization. However, in the case of the implementation of quantum gates, we have found that the optimal controls obtained from the unitary evolution exhibit a mean fidelity similar to that obtained from the non-unitary evolution. Since unitary optimization does not depend on decay rates nor on specific kinds of noise, besides being less computationally demanding, our results suggest that the best current practice to implement quantum gates in open quantum systems is to employ unitary optimization.

## I. INTRODUCTION

The ability to control quantum systems in the presence of environmental noise, which can lead to undesirable effects such as decoherence, is crucial for quantum computing [1–4]. There are many strategies to enhance the control of quantum systems in the presence of noise: decoherence-free subspaces [5–7], dynamical decoupling [8, 9], noiseless subsystems [10], and spectral engineering [11]. Although beneficial, these tactics are restricted to small systems and are typically limited to specific types of environment-system interactions.

Numerical optimal control becomes a particularly appealing method to deal with complicated systems and general forms of interactions [12–16]. In particular, the Krotov method (KM) has been extensively applied to the control of open systems [17–19]. In fact, cooperative effects of driving and dissipation have been demonstrated in the stochastic version of open quantum systems using the KM [17]. Moreover, the investigation of time-nonlocal non-Markovian master equation by means of the KM has shown a high fidelity implementation of a quantum gate for a qubit system depending on the control dissipation correlation and the memory effects related to the environment [18].

Here, we use the KM to perform state preparation from a known initial state as well as quantum gate implementation for both qubit and qutrit systems. We assume that the systems follow a Markovian master equation with either dephasing or amplitude-damping noise, which are standard archetypal of noisy channels [20]. Furthermore, we use two alternative ways to numerically obtain the

controls: (i) optimization in the presence of noise, which we refer to as non-unitary optimization, and (ii) optimization in the absence of noise, which we refer to as unitary optimization. We show that for the state preparation, the optimal control derived from non-unitary optimization outperforms unitary optimization. In the case of quantum gates, we discovered that non-unitary optimization outperforms unitary optimization only in one situation, and the difference in mean fidelity is negligible. This result is noteworthy since it shows that the optimal gate implementation for open systems can be found using unitary dynamics, which is independent of the decay rate and noise types.

## II. QUANTUM CONTROL APPLIED TO A QUANTUM SYSTEM WITH DISSIPATION

To consider a dissipative dynamics, we use the well-known Markovian master equation,

$$\frac{d\rho}{dt} = -\frac{i}{\hbar}[H, \rho] + D[\rho], \quad (1)$$

where the first term in the right hand side describes the unitary evolution and the second term includes the dissipation. Generally, the dissipator  $D[\rho]$  is given by

$$D[\rho] = \frac{\gamma}{2} \sum_j \left( 2L_j \rho L_j^\dagger - L_j^\dagger L_j \rho - \rho L_j^\dagger L_j \right), \quad (2)$$

where  $L_j$  are the Lindblad operators and  $\gamma$  is the decay rate, which we assume as a constant for all different Lindblad operators. The Hamiltonian  $H = H_0 + \varepsilon_\gamma(t)H_1$  can be divided into two terms, where the first term is the constant Hamiltonian  $H_0$  and the second term is composed by the product of the time-dependent control function

\* lkcastelano@df.ufscar.br

$\varepsilon_\gamma(t)$  and the Hamiltonian  $H_1$ . Since the optimization approach will be employed for each value of  $\gamma$ , as detailed below, the control function is dependent on the decay rate.

### III. KROTOV METHOD

Numerically, the optimal controls are sought by the Krotov method [12]. This method has been employed to study protocols related to standard-gate quantum computing with great efficiency [21]. The KM is an iterative monotonic approach for finding optimal controls that minimize a certain functional that is dependent on the control functions and the desired outcome. Here, we employ the same functional adopted in Ref. [12], which is given by

$$J_T = 1 - \sum_{i=0}^{n-1} \frac{w_i}{\text{Tr}[\rho_i^2(0)]} \text{Re} \left\{ \text{Tr} [O\rho_i(0)O^\dagger\rho_i(T)] \right\}, \quad (3)$$

where  $w_i$  is a weight for each initial state  $\rho_i(0)$ ,  $O$  is the desired unitary operation, and  $\rho_i(T)$  corresponds to the  $i$ -th initial state evolved up to the final time  $T$ . Within this formulation, one might consider a collection of  $n$ -initial states, each with a different weight, which can speed up the convergence of the KM. To obtain the control equations of the KM through variational calculus, a further constraint must be added

$$J = J_T - \int_0^T \frac{(\varepsilon_\gamma(t) - \varepsilon_\gamma^{ref}(t))^2}{\lambda S(t)} dt. \quad (4)$$

In the above equation,  $\lambda$  is a positive constant,  $\varepsilon_\gamma^{ref}(t)$  is a reference function, and  $S(t)$  is the envelope function. The extra constraint in Eq. (4) minimizes the fluence, which represents the integrated power transmitted from the control pulse to the system and its environment. Starting with a trial function  $\varepsilon_\gamma^0(t)$ , we need to self-consistently solve a set of coupled differential equations to find the correction for the control field  $\Delta\varepsilon_\gamma(t)$ . The first differential equation is related to the backward evolution (from the final time  $t = T$  to the initial time  $t = 0$ ) of the co-states  $\phi_i(t)$  through the following equation

$$\frac{\partial\phi_i^k(t)}{\partial t} = -\frac{i}{\hbar}[H^k, \phi_i^k] - D^\dagger[\phi_i^k], \quad (5)$$

where the subscript index  $i$  is related to the set of initial states that are being optimized,  $k$  indicates the  $k$ -th interaction of the self consistent calculation of the KM, while  $H^k = H_0 + \varepsilon_\gamma^k(t)H_1$ . Equation (5) is solved imposing a condition to the co-state at the final time, which is given by  $\phi_i^k(t = T) = \frac{w_i}{\text{Tr}[\rho_i^2(0)]} [O\rho_i(0)O^\dagger]$ . Additionally, the initial states  $\rho_i(0)$  are forward evolved according to the master equation,

$$\frac{d\rho_i^{k+1}(t)}{dt} = -\frac{i}{\hbar}[H^{k+1}, \rho_i^{k+1}] + D[\rho_i^{k+1}], \quad (6)$$

and the correction of the control function at the  $k$ -th interaction is

$$\varepsilon_\gamma^{k+1}(t) = \varepsilon_\gamma^k(t) + \lambda S(t)\Delta\varepsilon_\gamma^{k+1}(t) \quad (7)$$

where

$$\Delta\varepsilon_\gamma^{k+1}(t) = \text{Im} \left\{ \sum_{i=0}^{n-1} \text{Tr} \left\{ \phi_i^k(t) [H_1, \rho_i^{k+1}(t)] \right\} \right\}, \quad (8)$$

Equations (5-7) are solved in a self-consistent way and the value of the functional (Eq. 4) monotonically decreases.

### IV. RESULTS

To investigate the optimization of open quantum systems, we consider one qubit and one qutrit subjected to the noise of dephasing and amplitude-damping. The qubit Hamiltonian is  $H = H_0 + \varepsilon_\gamma(t)H_1$ , where  $H_0 = -\hbar\omega_0\sigma_z$  and  $H_1 = \hbar\omega_0\sigma_x$ . The Pauli spin matrices in the  $z$ - and  $x$ -direction are respectively denoted by  $\sigma_z$  and  $\sigma_x$ . The terms of the Hamiltonian describing the qutrit are

$$H_0 = -\hbar\omega_0 \begin{pmatrix} 1 & 0 & 0 \\ 0 & 0 & 0 \\ 0 & 0 & -1 \end{pmatrix}, \quad (9)$$

and

$$H_1 = \hbar\omega_0 \begin{pmatrix} 0 & 0 & 1 \\ 0 & 0 & 1 \\ 1 & 1 & 0 \end{pmatrix}. \quad (10)$$

Physically, a Hamiltonian with this kind of structure can be found when three electrons are confined in double quantum dots [22, 23] or in trapped ions [24]. To numerically solve the self-consistent equations (5-8), we first need to define some parameters. Thus, we adopt the time scale  $\tau = \omega_0^{-1}$  and the final evolution time  $T = 10\tau$ . Also, the initial guess for the control function is set up as  $\varepsilon_\gamma(t) = \varepsilon^0 S(t)$ , where  $\varepsilon^0$  is the initial amplitude of the trial function and  $S(t)$  is the envelope function that smoothly switches on and off the control function, given by

$$S(t) = \begin{cases} \sin^2\left(\frac{\pi t}{2t_r}\right), & \text{if } t \leq t_r \\ 1, & \text{if } t_r < t < T - t_r \\ \sin^2\left(\frac{\pi(t-T)}{2t_r}\right), & \text{if } t \geq T - t_r \end{cases} \quad (11)$$

In the above equation, we use  $\varepsilon^0 = 10^{-2}$  and  $t_r = T/30$ .

#### A. State preparation

First, we investigate the optimal control considering the case where an initial pure state described by

a density matrix  $\rho_0(0)$  is used to prepare a final state  $\rho_0(T) = O\rho_0(0)O^\dagger$ , where  $O$  is some particular quantum gate. For the qubit and the qutrit, we use  $\rho_0(0) = |0\rangle\langle 0|$ , where  $|0\rangle$  is the lowest energy level state. We employ the quantum Fourier transform for both qubit and qutrit as the quantum gate, which are respectively given by  $O = (\sigma_x + \sigma_z)/\sqrt{2}$  and

$$O = \frac{1}{\sqrt{3}} \begin{pmatrix} 1 & 1 & 1 \\ 1 & e^{2\pi i/3} & e^{4\pi i/3} \\ 1 & e^{4\pi i/3} & e^{8\pi i/3} \end{pmatrix}. \quad (12)$$

We find the optimal control function  $\varepsilon_\gamma^{opt}(t)$  for each decay rate  $\gamma$ . After obtaining the optimized control function, we perform the calculation of the fidelity, which is given by

$$F = \langle 0|O^\dagger\rho(T)O|0\rangle, \quad (13)$$

where  $\rho(T)$  is the solution of Eq. (1) at the final evolution time  $T$ . We use two different types of Lindblad operators, related to the dephasing channel and the amplitude-damping channel. For the qubit, the sum in Eq. (2) contains only the term  $j = 1$  and the Lindblad operator for dephasing is  $L_1 = \sigma_z$  whereas for amplitude-damping is  $L_1 = \sigma_-$ , where  $\sigma_- = (\sigma_x - i\sigma_y)/2$ . For the qutrit, the sum in Eq. (2) contains two terms  $j = 1, 2$  and the Lindblad operators for dephasing are  $L_1 = s_z^1$  and  $L_2 = s_z^2$  whereas for amplitude-damping are  $L_1 = s_-^1$  and  $L_2 = s_-^2$ , where  $s_z^1 = |1\rangle\langle 1| - |0\rangle\langle 0|$ ,  $s_z^2 = |2\rangle\langle 2| - |0\rangle\langle 0|$ ,  $s_-^1 = |1\rangle\langle 0|$ , and  $s_-^2 = |2\rangle\langle 0|$ . In Figures 1 and 2, we plot the fidelity for the dephasing (top panel) and amplitude-damping (bottom panel) as a function of the decay rate  $\gamma$  for a qubit and a qutrit, respectively. The blue dotted curves are obtained through the following steps: (i) find the optimized field  $\varepsilon_0^{opt}(t)$  for  $\gamma = 0$ ; (ii) plug this optimized field  $\varepsilon_0^{opt}(t)$  into Eq. (1) for each value of  $\gamma$ ; (iii) use the evolved density matrix at the final time to evaluate the fidelity of Eq. (13). The red solid curves in figures 1 and 2 are evaluated in a similar way, but the optimized field  $\varepsilon_\gamma^{opt}(t)$  is obtained for the corresponding value of  $\gamma$ , as explained in section II. For both qubits and qutrits, we can see that the fidelity obtained for the optimized function  $\varepsilon_\gamma^{opt}(t)$  evaluated for each value of  $\gamma$  is higher than the fidelity calculated with the unitary optimal function  $\varepsilon_0^{opt}(t)$ , as expected. When  $\gamma = 0.01$ , the fidelity for qubits considering the non-unitary optimal function is 3.5% and 0.26% higher than the one obtained with the unitary optimal function, respectively for the dephasing and amplitude-damping errors. For qutrits, the fidelity for qubits is 7% (dephasing) and 0.35% (amplitude-damping) higher for the non-unitary optimal function when  $\gamma = 0.01$ . Based on results of Figures 1 and 2, we conclude that the optimization considering the non-unitary optimization is more efficient to prepare a desired state for both qubit and qutrit; specially, for the qutrit subjected to dephasing.

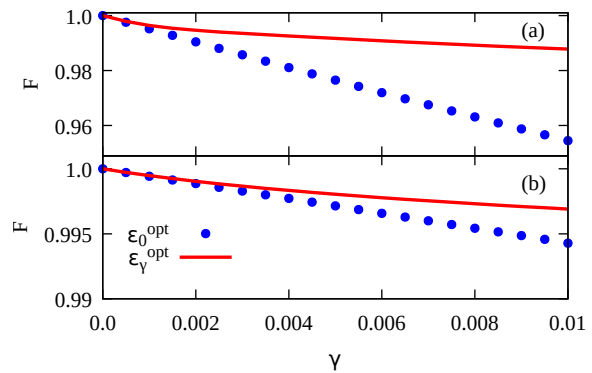


Figure 1. Fidelity for a qubit considering the dephasing (panel (a)) and the amplitude-damping (panel (b)) errors as a function of the decay rate  $\gamma$  using the optimized control function obtained from the unitary (blue dotted curve) and non-unitary dynamics (red solid curve).

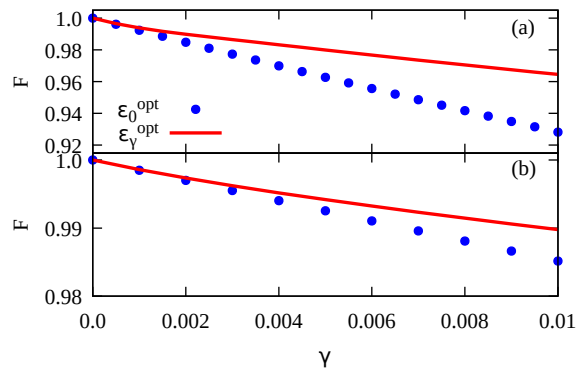


Figure 2. Fidelity for a qutrit considering the dephasing (panel (a)) and the amplitude-damping (panel (b)) errors as a function of the decay rate  $\gamma$  using the optimized control function obtained from the unitary (blue dotted curve) and non-unitary dynamics (red solid curve).

## B. Quantum gate

We consider the efficiency of the optimal functions when a quantum gate is the goal of the optimization. This situation is more subtle because the quantum gate should operate over an unknown initial state. To circumvent this situation, the optimization must take into account a set of initial states (for details, see Ref. [12]). For qubits, we employ the three initial states described in Refs. [25, 26], whose matrix elements are given by

$$\begin{aligned} \rho_j(0) &= |j\rangle\langle j| \text{ for } j=0,1 \\ \rho_2(0) &= \frac{1}{2} \sum_{i,j} |i\rangle\langle j|. \end{aligned} \quad (14)$$

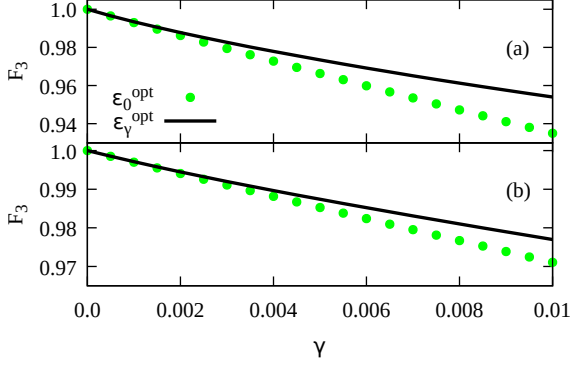


Figure 3. Three states fidelity for a qubit considering the dephasing (panel (a)) and the amplitude-damping (panel (b)) errors as a function of the decay rate  $\gamma$  using the optimized control function obtained from the unitary (green dotted curve) and non-unitary dynamics (black solid curve).

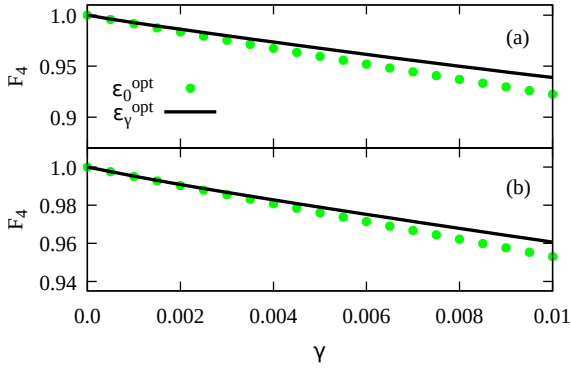


Figure 4. Four states fidelity for a qutrit considering the dephasing (panel (a)) and the amplitude-damping (panel (b)) errors as a function of the decay rate  $\gamma$  using the optimized control function obtained from the unitary (green dotted curve) and non-unitary dynamics (black solid curve).

For qutrits, we use the following four initial states [23],

$$\begin{aligned} \rho_j(0) &= |j\rangle\langle j| \text{ for } j=0,1,2 \\ \rho_3(0) &= \frac{1}{3} \sum_{i,j} |i\rangle\langle j|. \end{aligned} \quad (15)$$

The weights in Eq. (4) are assumed to be  $w_j = 1/N$  (unless specified), where  $N=3$  for the qubit and  $N=4$  for the qutrit. First, we analyze the efficiency of the KM to improve the set of initial states. To probe this efficiency, we employ the mean fidelity over all initial states defined as

$$F_n = \frac{1}{n} \sum_{i=1}^n \left\{ \text{Tr} \sqrt{\sqrt{\sigma} \rho_i(T) \sqrt{\sigma}} \right\}^2, \quad (16)$$

where  $\sigma = O\rho_i(0)O^\dagger$ . Figures 3 and 4 show the mean fidelity over initial states for the dephasing (panel (a)) and

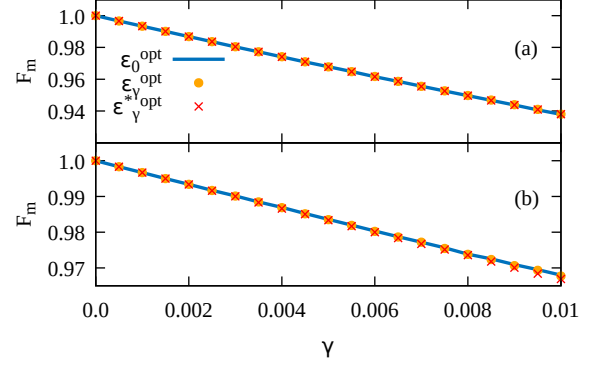


Figure 5. Mean fidelity for a qubit considering the dephasing (panel (a)) and the amplitude-damping (panel (b)) errors as a function of the decay rate  $\gamma$  using the optimized control function obtained from the unitary (orange dotted curve) and non-unitary dynamics (blue solid curve).

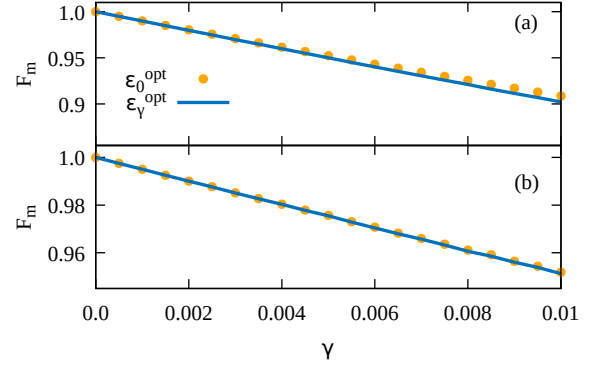


Figure 6. Mean fidelity for a qutrit considering the dephasing (panel (a)) and the amplitude-damping (panel (b)) errors as a function of the decay rate  $\gamma$  using the optimized control function obtained from the unitary (orange dotted curve) and non-unitary dynamics (blue solid curve).

the amplitude-damping (panel (b)) as a function of the decay rate  $\gamma$ , respectively for the qubit and the qutrit. The green dotted curve is obtained for  $\varepsilon_0^{opt}(t)$  and evolving the Eq. (1) considering the initial states for the qubit Eq. (14) and for the qutrit Eq. (15). The evolved density matrices are used to evaluate the mean fidelity of equation Eq. (16) for each value of  $\gamma$ . The black solid curves in Figures 3 and 4 are evaluated in a similar way, but the employed optimized function  $\varepsilon_\gamma^{opt}(t)$  is different for each value of  $\gamma$ . In both Figures, one can see that the mean fidelity obtained for the non-unitary optimization surpass the unitary optimization, which numerically shows that the KM is improving the non-unitary control to achieve a higher fidelity for the set of initial states.

To probe the efficiency of the implementation of the

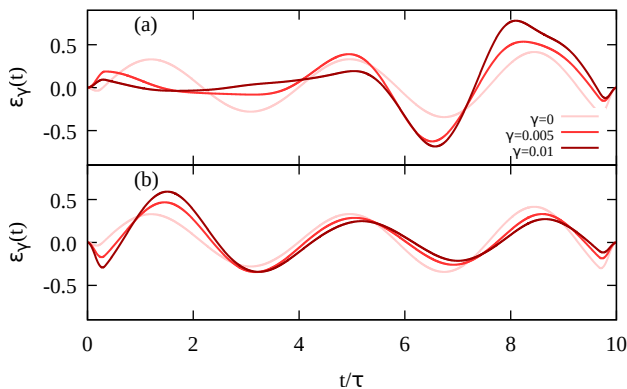


Figure 7. Optimal control functions obtained for a quantum gate implementation for a qubit considering the dephasing (panel (a)) and the amplitude-damping (panel (b)) for different values of the decay rate  $\gamma$ .

quantum gate, we use the mean fidelity given by

$$F_m = \frac{1}{N_s} \sum_{i=1}^{N_s} \langle \varphi_i | O^\dagger \rho(T) O | \varphi_i \rangle, \quad (17)$$

where  $|\varphi_i\rangle$  is a pure random state. The ensemble of pure random matrices  $|\varphi_i\rangle\langle\varphi_i|$  is built in such a way that all states are uniformly distributed according to the Hilbert-Schmidt norm [27].

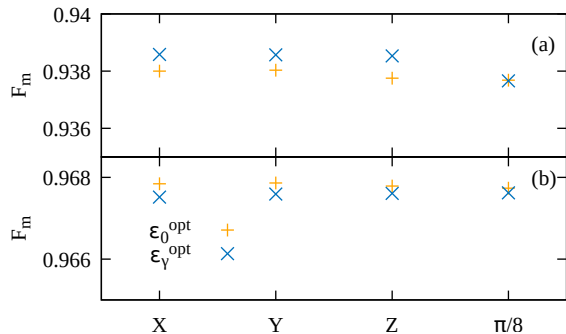


Figure 8. Panels (a) and (b) refer to the errors dephasing and amplitude-damping, respectively. The results for the mean fidelity for a fixed value of the decay rate  $\gamma = 0.01$  considering one qubit quantum gates  $X$ ,  $Y$ ,  $Z$  and  $\pi/8$  using the optimized control function obtained from the unitary (orange symbols) and non-unitary dynamics (blue symbols).

Figure 5 and 6 show the mean fidelity for the dephasing (panel (a)) and amplitude-damping (panel (b)) as a function of the decay rate  $\gamma$ , respectively for the qubit and the qutrit. The orange dotted curve is obtained for  $\varepsilon_0^{opt}(t)$  and evolving the Eq. (1) considering  $N_s = 12^4$  initial states. The evolved density matrices are used to evaluate the mean fidelity of equation (13) for each value of  $\gamma$ . The blue solid curves in Figures 5 and 6 are eval-

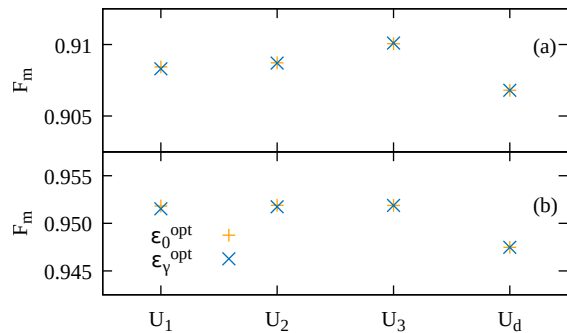


Figure 9. Panels (a) and (b) refer to the errors dephasing and amplitude-damping, respectively. The results for the mean fidelity for a fixed value of the decay rate  $\gamma = 0.01$  considering one qutrit quantum gates  $U_1$ ,  $U_2$ ,  $U_3$  and  $U_d$ , as defined in the main text. We compare the optimized control function obtained from the unitary (orange symbols) and non-unitary dynamics (blue symbols).

uated considering the function  $\varepsilon_\gamma^{opt}(t)$ , which are optimized for each value of  $\gamma$ . In both figures 5 and 6, one can see that the mean fidelity obtained for the unitary and non-unitary control functions considering both type of errors are essentially the same, although the optimized control functions are distinct for different values of the decay rate (see Fig. 7). For the qubit, we also add a result for the mean fidelity considering different initial states proposed in ref. [12], which are given by  $\rho_0(0) = 2/3|0\rangle\langle 0| + 1/3|1\rangle\langle 1|$ ,  $\rho_1(0) = 1/2(|0\rangle + |1\rangle)(\langle 0| + \langle 1|)$ , and  $\rho_2(0) = 1/2|0\rangle\langle 0| + 1/2|1\rangle\langle 1|$ . For this case, we employ the weights in Eq. (3) as  $w_0 = 8w_1$  and  $w_1 = w_2$ . The mean fidelity evaluated for the non-unitary control function  $\varepsilon_\gamma^{*opt}(t)$ , considering these initial states, is also shown in figure 5 by the red crosses, but one can observe that the result for the mean fidelity is very similar to the one found considering  $\varepsilon_0^{opt}(t)$ .

These results are counter intuitive because it was expected that the optimal function  $\varepsilon_\gamma^{opt}(t)$  would improve the mean fidelity evaluated with the unitary optimization  $\varepsilon_0^{opt}(t)$ , as previously observed for the initial states mean fidelity. To further investigate this scenario, we consider four different types of quantum gates and evaluate the mean fidelity considering  $\gamma = 0.01$ . Such results are shown in figures 8 and 9. In figure 8, we plot the mean fidelity for qubits considering the following quantum gates:  $X = \sigma_x$ ,  $Y = \sigma_y$ ,  $Z = \sigma_z$ , and  $\pi/8 = |0\rangle\langle 0| + e^{i\pi/4}|1\rangle\langle 1|$ . When the dephasing channel is taking into account (Fig. 8(a)), the mean fidelity evaluated with the non-unitary control is higher than the one evaluated with the unitary control for the gates  $X$ ,  $Y$ , and  $Z$ , but the gain is very small of the order of 0.05%. On the other hand, the non-unitary optimization provides a less efficient mean fidelity for the amplitude-damping chan-

nel. For qutrits, we use the following quantum gates [24]:

$$U_1 = \frac{1}{\sqrt{2}} \begin{pmatrix} 1 & -e^{-2\pi i/3} & 0 \\ -e^{2\pi i/3} & -1 & 0 \\ 0 & 0 & -\sqrt{2} \end{pmatrix}, \quad (18)$$

$$U_2 = \frac{1}{\sqrt{2}} \begin{pmatrix} 1 & 0 & ie^{2\pi i/3} \\ 0 & \sqrt{2} & 0 \\ ie^{-2\pi i/3} & 0 & 1 \end{pmatrix}, \quad (19)$$

$$U_3 = \frac{1}{\sqrt{3}} \begin{pmatrix} \sqrt{3} & 0 & 0 \\ 0 & -\sqrt{2} & ie^{-\pi i/6} \\ 0 & ie^{\pi i/6} & -\sqrt{2} \end{pmatrix}, \quad (20)$$

and

$$U_d = \begin{pmatrix} e^{\pi i/3} & 0 & 0 \\ 0 & e^{\pi i/6} & 0 \\ 0 & 0 & e^{-\pi i/2} \end{pmatrix}. \quad (21)$$

We use the same Hamiltonian described in section IV for the qubit, but we have to alter  $H_1$  for implementing the gates above for the qutrit. Basically, we have used the matrix elements of  $H_1$  equal to one in the same position where the quantum gate has a matrix element different from zero. In both panels of figure 9, we can observe that the non-unitary and the unitary present an almost identical value for the mean fidelity. These results show

that the unitary optimal control function  $\varepsilon_0^{opt}(t)$  is a solution very close to the optimal solution to implement a quantum gate for open quantum systems described by the Markovian master equation in Eq.(1).

## V. CONCLUSION

In this work we used the KM for open and closed quantum systems to investigate state preparation and quantum gate implementation. The optimal control function derived by the non-unitary KM is shown to benefit state preparation. The quantum gate implementation, on the other hand, has almost identical mean fidelity for the unitary and non-unitary optimal control functions. This implies that the KM for an open quantum system is not more efficient than the KM for a closed quantum system. The non-unitary KM is unable of creating an optimal control function to operate over all states at the same time since the quantum gate must act over arbitrary input states. As a result, the unitary KM's optimal control function has a similar efficiency to that of the non-unitary KM's. This finding is intriguing since the unitary optimal control functions need only be determined for unitary dynamics and are independent of the decay rate magnitude. The present results also indicates that the development of novel techniques for improving the non-unitary KM's optimal functions deserves further exploration.

- 
- [1] Z. An, H.-J. Song, Q.-K. He, and D. L. Zhou, Phys. Rev. A **103**, 012404 (2021), URL <https://link.aps.org/doi/10.1103/PhysRevA.103.012404>.
- [2] L. C. Venuti, D. D'Alessandro, and D. A. Lidar, Phys. Rev. Applied **16**, 054023 (2021).
- [3] C. P. Koch, Journal of Physics: Condensed Matter **28**, 213001 (2016), URL <https://doi.org/10.1088/0953-8984/28/21/213001>.
- [4] R. Roloff, M. Wenin, and W. Pötz, Journal of Computational and Theoretical Nanoscience **6**, 1837 (2009), ISSN 1546-1955, URL <https://www.ingentaconnect.com/content/asp/jctn/2009/00000006/00000008/art00008>.
- [5] D. A. Lidar, I. L. Chuang, and K. B. Whaley, Phys. Rev. Lett. **81**, 2594 (1998), URL <https://link.aps.org/doi/10.1103/PhysRevLett.81.2594>.
- [6] L.-A. Wu, P. Zanardi, and D. A. Lidar, Phys. Rev. Lett. **95**, 130501 (2005), URL <https://link.aps.org/doi/10.1103/PhysRevLett.95.130501>.
- [7] P. G. Kwiat, A. J. Berglund, J. B. Altepeter, and A. G. White, Science **290**, 498 (2000), <https://www.science.org/doi/pdf/10.1126/science.290.5491.498>, URL <https://www.science.org/doi/abs/10.1126/science.290.5491.498>.
- [8] L. Viola, E. Knill, and S. Lloyd, Phys. Rev. Lett. **82**, 2417 (1999), URL <https://link.aps.org/doi/10.1103/PhysRevLett.82.2417>.
- [9] A. M. Souza, G. A. Álvarez, and D. Suter, Phys. Rev. Lett. **106**, 240501 (2011), URL <https://link.aps.org/doi/10.1103/PhysRevLett.106.240501>.
- [10] L. Viola, E. M. Fortunato, M. A. Pravia, E. Knill, R. Laflamme, and D. G. Cory, Science **293**, 2059 (2001).
- [11] J. Clausen, G. Bensky, and G. Kurizki, Phys. Rev. Lett. **104**, 040401 (2010), URL <https://link.aps.org/doi/10.1103/PhysRevLett.104.040401>.
- [12] M. H. Goerz, D. M. Reich, and C. P. Koch, New Journal of Physics **16**, 055012 (2014), URL <https://doi.org/10.1088/1367-2630/16/5/055012>.
- [13] H. Ball, M. J. Biercuk, A. R. R. Carvalho, J. Chen, M. Hush, L. A. D. Castro, L. Li, P. J. Liebermann, H. J. Slatyer, C. Edmunds, et al., Quantum Science and Technology **6**, 044011 (2021), URL <https://doi.org/10.1088/2058-9565/abdca6>.
- [14] A. Levy, E. Torrontegui, and R. Kosloff, Phys. Rev. A **96**, 033417 (2017), URL <https://link.aps.org/doi/10.1103/PhysRevA.96.033417>.
- [15] M. Y. Niu, S. Boixo, V. N. Smelyanskiy, and H. Neven, npj Quantum Information **5**, 33 (2019), ISSN 2056-6387, URL <https://doi.org/10.1038/s41534-019-0141-3>.
- [16] A. Levy, A. Kiely, J. G. Muga, R. Kosloff, and E. Torrontegui, New Journal of Physics **20**, 025006 (2018), URL <https://doi.org/10.1088/1367-2630/aaa9e5>.
- [17] R. Schmidt, A. Negretti, J. Ankerhold, T. Calarco, and J. T. Stockburger, Phys. Rev. Lett. **107**,

- 130404 (2011), URL <https://link.aps.org/doi/10.1103/PhysRevLett.107.130404>.
- [18] B. Hwang and H.-S. Goan, *Phys. Rev. A* **85**, 032321 (2012), URL <https://link.aps.org/doi/10.1103/PhysRevA.85.032321>.
- [19] Y. Chou, S.-Y. Huang, and H.-S. Goan, *Phys. Rev. A* **91**, 052315 (2015), URL <https://link.aps.org/doi/10.1103/PhysRevA.91.052315>.
- [20] K. M. F. Romero and R. L. Franco, *Physica Scripta* **86**, 065004 (2012), URL <https://doi.org/10.1088/0031-8949/86/06/065004>.
- [21] J. P. Palao and R. Kosloff, *Phys. Rev. Lett.* **89**, 188301 (2002), URL <https://link.aps.org/doi/10.1103/PhysRevLett.89.188301>.
- [22] Z. Shi, C. B. Simmons, D. R. Ward, J. R. Prance, X. Wu, T. S. Koh, J. K. Gamble, D. E. Savage, M. G. Lagally, M. Friesen, et al., *Nature Communications* **5**, 3020 (2014), ISSN 2041-1723, URL <https://doi.org/10.1038/ncomms4020>.
- [23] C. M. Rivera-Ruiz, E. F. de Lima, F. F. Fanchini, V. Lopez-Richard, and L. K. Castelano, *Phys. Rev. A* **97**, 032332 (2018), URL <https://link.aps.org/doi/10.1103/PhysRevA.97.032332>.
- [24] A. B. Klimov, R. Guzmán, J. C. Retamal, and C. Saavedra, *Phys. Rev. A* **67**, 062313 (2003), URL <https://link.aps.org/doi/10.1103/PhysRevA.67.062313>.
- [25] C. M. Tesch and R. de Vivie-Riedle, *The Journal of Chemical Physics* **121**, 12158 (2004), <https://aip.scitation.org/doi/pdf/10.1063/1.1818131>, URL <https://aip.scitation.org/doi/abs/10.1063/1.1818131>.
- [26] J. P. Palao and R. Kosloff, *Phys. Rev. A* **68**, 062308 (2003), URL <https://link.aps.org/doi/10.1103/PhysRevA.68.062308>.
- [27] H.-J. Sommers and K. Zyczkowski, *Journal of Physics A: Mathematical and General* **37**, 8457 (2004), URL <https://doi.org/10.1088/0305-4470/37/35/004>.